Computers and Chemical Engineering 149 (2021) 107289

Contents lists available at ScienceDirect

Computers and Chemical Engineering

journal homepage: www.elsevier.com/locate/compchemeng

Investigation of the chemical vapor deposition of Cu from copper amidinate through data driven efficient CFD modelling

R. Spencer[a], P. Gkinis[b], E.D. Koronaki[b,c,*], D.I. Gerogiorgis[a], S.P.A. Bordas[c], A.G. Boudouvis[b]

[a] Institute for Materials and Processes (IMP), School of Engineering, University of Edinburgh, The King's Buildings, Edinburgh EH9 3FB, United Kingdom
[b] School of Chemical Engineering, National Technical University of Athens, 9 Heroon Polytechniou str, Zographos Campus, 15780, Greece
[c] Faculté des Sciences, de la Technologie et de la Communication, Université de Luxembourg, Maison du Nombre, Avenue de la Fonte 6, L-4364 Esch-sur-Alzette, Luxembourg

ARTICLE INFO

Article history:
Received 25 January 2021
Revised 11 March 2021
Accepted 13 March 2021
Available online 16 March 2021

Keywords:
Copper amidinate
Chemical Vapor Deposition
Reduced-order modeling
Data-driven model
Chemical reaction pathway

ABSTRACT

A chemical reaction model, consisting of two gas-phase and a surface reaction, for the deposition of copper from copper amidinate is investigated, by comparing results of an efficient, reduced order CFD model with experiments. The film deposition rate over a wide range of temperatures, 473K-623K, is accurately captured, focusing specifically on the reported drop of the deposition rate at higher temperatures, i.e above 553K that has not been widely explored in the literature. This investigation is facilitated by an efficient computational tool that merges equation-based analysis with data-driven reduced order modeling and artificial neural networks. The hybrid computer-aided approach is necessary in order to address, in a reasonable time-frame, the complex chemical and physical phenomena developed in a three-dimensional geometry that corresponds to the experimental set-up. It is through this comparison between the experiments and the derived simulation results, enabled by machine-learning algorithms that the prevalent theoretical hypothesis is tested and validated, illuminating the possible underlying dominant phenomena.

1. Introduction

In process analysis and design, data-driven methods are considered as the new paradigm that can lead to increased insight by leveraging various types of data (Clayton et al., 2020; Zhu et al., 2021; Yan et al., 2020; Bracconi and Maestri, 2020; Narasingam and Sang-Il Kwon, 2018; Stluka and Mařík, 2007; Koronaki et al., 2019; Koronaki et al., 2020; Alshehri, 2020; Lee et al., 2018; Koo et al., 2019). Nevertheless, in recent years, equation-based analysis has reached the point of remarkable accuracy, by efficiently combining transport phenomena simulations and chemical reactions into a single predictive model (Koo et al., 2019; Shi et al., 2021; Lira et al., 2020; Gyurik et al., 2020; Massmann et al., 2020; Chen et al., 2020; Kim et al., 2020; Gao et al., 2020; Chen et al., 2020; Gosiewski and Pawlaczyk-Kurek, 2019). In this work, data-driven methods are applied in conjunction with equation-based models for additional benefits in terms of accuracy and efficiency, in the study of the Chemical Vapor Deposition (CVD) of copper (Cu) from Cu amidinate.

The CVD of copper has emerged as an attractive process for the replacement of aluminum by Cu in integrated circuits due to the latter's low resistance, high thermal and electrical conductivity (Prud'homme et al., 2020; Rasadujjaman et al., 2015; Mwema et al., 2018; Tanaka et al., 2001). Extensive research in this field strives to improve deposition conformality, film uniformity and surface roughness and to relate these characteristics to the parameters of the process, namely the deposition temperature, the chamber pressure, the mass-flow rate and consistency of the reactive gas mixture. Research also focuses on new precursors (Mayangsari et al., 2021; Sharif and Ahmad, 2020; Nishikawa et al., 2020; Panzeri et al., 2019) in an effort to improve the throughput of the process and the quality of the deposited metal, while reducing energy consumption and the involvement of dangerous raw materials and by-products.

The constant need to adapt and evolve processes to meet the current process and product quality requirements, given the progress in precursor and material design, requires efficient and accurate investigative workflows that are able to quickly propose viable modifications in the process. In this effort, predictive and design tools that are accurate and easily adaptable are gaining momentum. Nevertheless, the cost associated with the development and application of the predictive models is significant, rendering the multi-parametric investigation a time- and resource- consuming task. The answer to this problem is given by data-mining in the form of the popular Proper Orthogonal Decomposition (POD)

* Corresponding author.
E-mail address: ekor@mail.ntua.gr (E.D. Koronaki).

https://doi.org/10.1016/j.compchemeng.2021.107289
0098-1354/

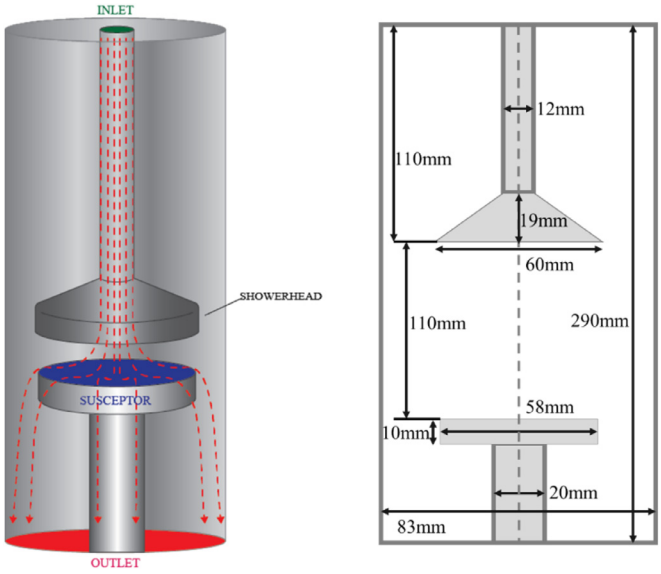

Fig. 1. Schematic illustration of the experimental MOCVD reactor.

method (Sipp et al., 2020; Wang et al., 2020; Li et al., 2019; Hijazi et al., 2020; Dey and Dhar, 2020), that has led to model order reduction strategies by discovering low-order descriptions of the available data, i.e. an orthogonal basis of the subspace containing the data.

This work presents the implementation of a hybrid workflow that hinges equation-based and data-mining methodologies, as a means of identifying a chemical pathway for the deposition of Cu from Cu amidinate (N,N-diisopropylacetamidinate or $[Cu(amd)]_2$), that is valid over a wide temperature range. Despite the popularity of $[Cu(amd)]_2$ as a precursor (Krisyuk et al., 2009), a deposition model that is valid across a wide temperature range is still lacking. This precursor typically provides higher purity solid Cu films due to its lack of halogens and oxygen, at relatively lower deposition temperatures (approximately 473K) compared to similar precursors. Experimental measurements, available in the literature will be used to calibrate the proposed model ensuring accuracy. Efficiency will be achieved by exploiting low-fidelity data, produced at a low computational cost, in order to first derive a low-fidelity/high-efficiency predictive model. The results of these models will be used as initial approximations for detailed, or high-fidelity models, ensuring their faster convergence.

The rest of the paper is organized as follows: The CVD case is presented, providing details on the geometry, experimental conditions and reactive gas mixture composition. This is followed by a literature review of Cu deposition pathways, that lays the foundation for the deposition model. The computational workflow is then presented, starting from the equation-based component and proceeding to the data-driven workflow, followed by results and conclusions.

2. Case study

The case study here, is the vertical cylindrical MOCVD reactor with stainless steel walls, used in the experimental set up described in (Krisyuk et al., 2009), shown in Fig. 1. In this reactor configuration, a showerhead ensures homogeneous distribution of the reactive gases over the heated stainless steel susceptor. In addition to the experiments presented in (Krisyuk et al., 2009), experimental measurements in the same reactor, in two higher susceptor temperatures, 593K and 623K, are made available (C. Vahlas, personal communication, 2020). For details concerning the experimental set-up and conditions, the interested reader in referred to (Krisyuk et al., 2009) for and in-depth presentation. The data are summarized collectively in an Arrhenius plot of the deposition rate with respect to the inverse of the susceptor temperature shown in Fig. 2. The deposition rate is computed experimentally by weight difference of the substrate, before and after deposition. Three independent weight measurements, pre and post experiment are taken for each substrate and the average value is reported in Fig. 2. This is repeated for different susceptor temperatures while the rest of the reactor conditions fixed. The latter are listed in Table 1.

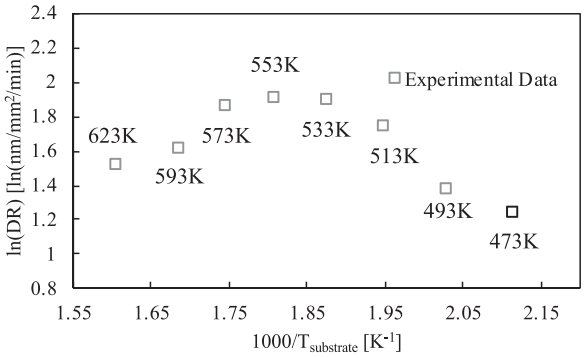

Fig. 2. Arrhenius plot (deposition rate vs inverse of substrate temperature) of Cu deposition from Cu amidinate.

Table 1
Experimental operating conditions and gas mixture conditions.

Experimental Conditions	
Pressure (Pa)	1333
Reactor walls temperature (K)	368
Substrate temperature (K)	473, 493, 513, 533, 553, 573, 593, 623
Gas mixture	
Inlet temperature (K)	368
Inlet mass flowrate (kg/s)	$7.47 \cdot 10^{-6}$
Mass fractions	
$[Cu(amd)]_2$	0.001016
H_2	0.004107
N_2	0.2556
Ar	0.739277

Table 2
Boundary conditions of the 3D-CFD reactor model.

Boundary	Conditions
Walls	Stationary No slip Temperature - 368K
Inlet	Mass inlet flow – $7.473 \cdot 10^{-6}$kg/s Initial gauge pressure – 0 Pa Temperature – 368 K Species mass fractions (Table 1)
Susceptor	Stationary No slip Temperature – 473-623K
Outlet	Outflow

3. Proposed chemical reaction model

The composition and reactivity of the gas phase during the MOCVD process of copper amidinate, is studied in (Turgambaeva et al., 2011) using mass spectrometry. It is suggested that in the presence of hydrogen, the only significant reaction is

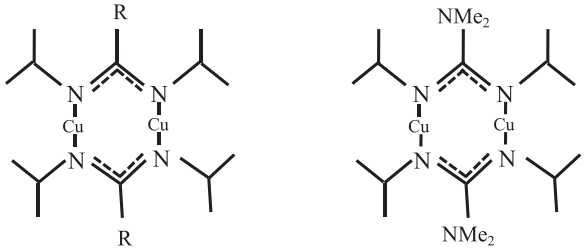

Fig. 3. Copper amidinate (left) vs copper guanidinate (right).

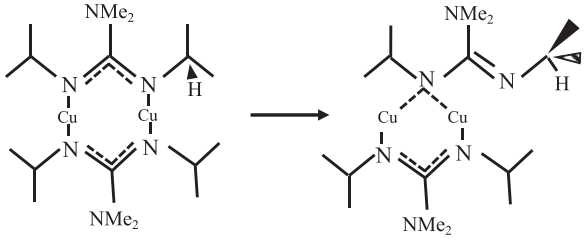

Fig. 4. Ligand shift for copper (I) Guanidinate.

the following surface reaction:

$$[Cu(amd)]_{2(g)} + H_{2(g)} \rightarrow 2Cu_{(s)} + 2H(amd)_{(g)} \quad (S1)$$

The activation energy is estimated based on the available experiments, in the reaction limited regime, i.e. at low deposition temperatures where the reaction rate is expected to be the dominant rate-defining mechanism. As shown in Fig. 2, there is an almost linear increase of the deposition rate with respect to temperature, for deposition temperatures lower than 533K, signifying that the reaction is the rate-limiting step in the deposition process. Given that an Arrhenius type kinetic is adopted for the reaction rate, the activation energy of the surface reaction, derived as the slope of the curve in this reaction-limited regime, is found to be 66 kJ/mol. This value is in good agreement with the one mentioned in Lim (2003), where they defined it as 60 kJ/mol.

Nevertheless, the experiments described in (Turgambaeva et al., 2011) were only carried out at temperatures up to 573K. Later experimental findings (Aviziotis et al., 2013) indicate that there is a notable reduction of Cu deposition rate past 573K (cf. Fig. 2), signifying possibly the depletion of precursor or a similar growth limiting phenomenon. In the following literature review, possible chemical pathways are presented aiming to identify the candidate that is more likely to capture the decrease in the deposition rate above 573K.

Gas phase nucleation or a volumetric decomposition reaction activated at high temperatures are possible reasons for the decrease of the deposition rate at higher temperatures. The former is not considered as a likely candidate, because typically particles would be observed on the reactor walls as a result of the nucleation reaction. Based on the literature and also on in-house experimental expertise, Cu particles are not reported even in high deposition temperatures. Therefore, the effect of volumetric decomposition is considered as more probable, based also on previous findings from the study of the decomposition of metallic precursors with amidinate and amidinate-type ligands by Barry (2013). The study suggests two different pathways for the decomposition of the copper amidinate, either by elimination of the carbodiimide or by abstraction of β-hydrogen. The first is preferable for lower temperature solution-based thermolysis and the second takes place in higher temperatures and gas-phase systems. These two pathways are also suggested by Coyle et al. (2010) in a study of copper guanidinate, a structurally similar precursor to copper amidinate; said similarity is shown in Fig.. 3 with the structures of each compound side by side. In fact, this similarity is also suggested by Barry (2013).

Two decomposition pathways are proposed in the literature (Barry, 2013; Coyle et al., 2012) both based on an initial endothermic ligand shifting, as illustrated in Fig. 4. Ligand shifting for guanidinate has an activation energy of 94.1kJ mol^{-1}, which in the absence of numerical data for amidinate is assumed to be identical for the latter due to their highly similar structures. This activation energy is significantly higher than the one required for the surface deposition reaction of Cu, thus is consistent with the idea of a high-temperature activated decomposition reaction taking place in this process. After the ligand shift, the new geometry allows for both the carbodiimide deinsertion and β-hydrogen abstraction to occur. These subsequent pathways and their respective activation energies are shown in Fig. 5.

In the gas phase both pathways can occur, but it is possible that β-hydrogen abstraction is predominant due to surface-activated mechanisms (Barry, 2013). In the absence of information on which of the two subsequent pathways actually prevails, both are adopted in the model and fitted on the experimental results with identical pre-exponential factors. Thus, the model is not relying on one, or mainly one of the two decomposition reactions to describe the decreasing deposition rate at high temperatures, making the model flexible for future optimization.

In summary, in addition to the surface reaction (S1), the following two decomposition reactions of copper amidinate are included: (a) the carbodiimide deinsertion and (b) the β-hydrogen abstraction.

$$[Cu(amd)]_{2(g)} \rightarrow 2Cu(CH_3)_{2(g)} + 2CH(CH_3)_2\text{-NCN-}CH(CH_3)_{2(g)} \quad (G1)$$

$$[Cu(amd)]_{2(g)} \rightarrow 2CuH_{(g)} + 2CH(CH_3)_2\text{-N=C}(CH_3)\text{-N=C}(CH_3)_{2(g)} \quad (G2)$$

4. CFD modeling

The reactor is represented by a three-dimensional (3D) geometry in order to account for the effect of the showerhead in the distribution of species and the development of the flow. The time-dependent transport equations for mass, momentum and energy are discretized with the finite volume method with 1.2 M finite volumes and solved in ANSYS/Fluent (Koronaki et al., 2019; Gkinis et al., 2017a; Gkinis et al., 2017; Gkinis et al., 2019). Concerning the boundary conditions, for the velocity: at the inlet of the reactor a constant mass inflow rate of 7.473 $\times$ 10^{-6}kg/s is imposed, calculated from the total volumetric flow of the mixture. No-slip condition is imposed at all the walls of the reactor. At the outlet, a standard outflow boundary condition is used. At the susceptor the temperature varies, between 473-623 K based on the experimental conditions described in (Krisyuk et al., 2009). For the species: the mass fractions of the species entering the reactor are summarized in Table 1. The flux of all species at the reactor walls is zero except on the substrate where the surface reactions (deposition) take place. An overall mass balance correction is imposed at the outlet. The operating pressure of the reactor is 1333 Pa.

The properties of the individual species and of the mixture are computed as in Aviziotis et al. (2013). The Lennard-Jones (LJ) parameters, namely σ and ε, are the parameters of the LJ potential and are needed for the estimation of the properties in the gas phase of the CVD reactor. σ is the measure of the size of the molecules and ε/k is a measure of how strongly the molecules attract each other. For the unknown species, namely $[Cu(amd)]_2$ and H(amd), their values are calculated with group contribution methods [18] and for $[Cu(amd)]_2$ are: σ= 10.8525Å and ε/k =423.2 K and for H(amd): σ= 9.4874Å and ε/k = 534.8 K.

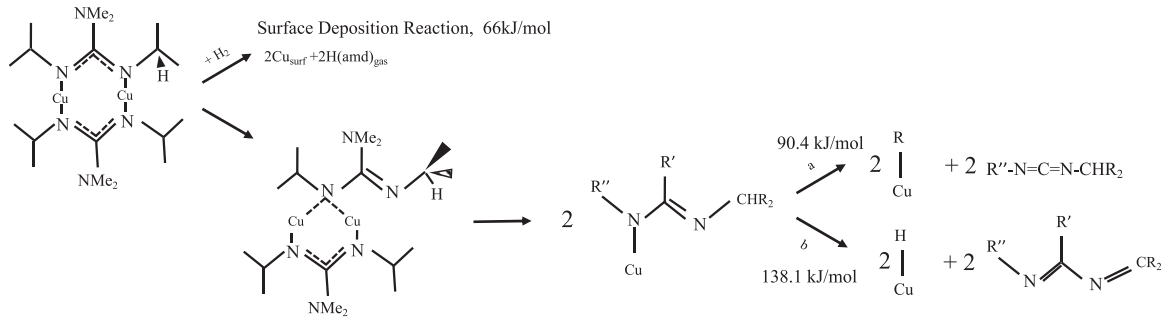

Fig. 5. Potential decomposition pathways for copper amidinate; pathway (a) carbodiimide deinsertion, pathway (b) β-hydrogen abstraction.

The effect of the chemical reactions is included, specifically as a second order bimolecular elementary and a first order elementary rate law, for the surface (S1) and the gas phase decomposition reactions (G1, G2) respectively. The kinetic constants for these reactions are fitted simultaneously based on the experimental findings,

$$\text{Deposition rate (DR)} = k_0 \exp\left(-\frac{66\text{kJ/mol}}{RT}\right) C_{[Cu(amd)]_2} C_{H_2} \quad \text{(S1)}$$

$$\text{Reaction rate (RR)} = k_1 \exp\left(-\frac{90.4\text{kJ/mol}}{RT}\right) C_{[Cu(amd)]_2} \quad \text{(G1)}$$

$$\text{Reaction rate (RR)} = k_2 \exp\left(-\frac{138.1\text{kJ/mol}}{RT}\right) C_{[Cu(amd)]_2} \quad \text{(G2)}$$

Here k_0, k_1 and k_2 are pre-exponential factors, R the universal gas constant, T the temperature, $C_{[Cu(amd)]2}$ and C_{H2} the molecular concentrations, in kmol/cm^3, of amidinate and hydrogen respectively. As mentioned in section 3, the activation energy for the surface reaction is calculated based on the deposition experiments reported in Fig. 2, whereas for the gas-phase reactions, the activation energies for the carbodiimide deinsertion and the β-hydrogen abstraction of Cu guanidinate is adopted here, for lack of data about the amidinate decomposition.

The complete, 3D CFD model that includes the three chemical reactions and the conservation equations for all the participating species, has over 16 million degrees of freedom. Each simulation requires about 72 CPU hours on 12 cores, i.e. 72 × 12 = 864 core hours. This amounts to significant computational effort, considering that several parameter values are explored during the fitting procedure, in order to determine the pre-exponential factors with a trial-and-error approach: CFD predictions, using assumed k_0, k_1 and k_2 values are compared to experimental measurements and are recursively adjusted until the experiments are captured with satisfactory accuracy. The need naturally arises for the implementation of an efficient model order reduction strategy that will enable the aforementioned parametric investigation.

5. Reduced Order Model development

The workflow presented here, consists of a Reduced Order Model and a detailed, fine-mesh model that incorporates chemical reactions and species conservation equations. The goal of the ROM is to predict a good enough approximation of the flow field and temperature distribution for any given set of process parameters. This coarse, in terms of accuracy, approximation is then used as initial guess in the detailed CFD model and enables it to converge at a lower computational cost than it would have done if it were initialized from a generic initial guess. The ROM is oblivious of the chemistry model as it is built using snapshots from a low-fidelity CFD model, involving a coarse discretization, without chemical reactions. This course of action is pursued in order to keep the computational effort involved in developing the ROM as small as possible, while still generating an approximation of the solution that is close to the actual. This solution can then be used in order to initialize the detailed CFD model for various different values of the kinetic parameters allowing it to converge faster. The latter is made possible by the fact that the mixture of gas reactants is dilute and therefore the depletion of precursor and the production of new species does not affect the development of the flow and temperature distribution.

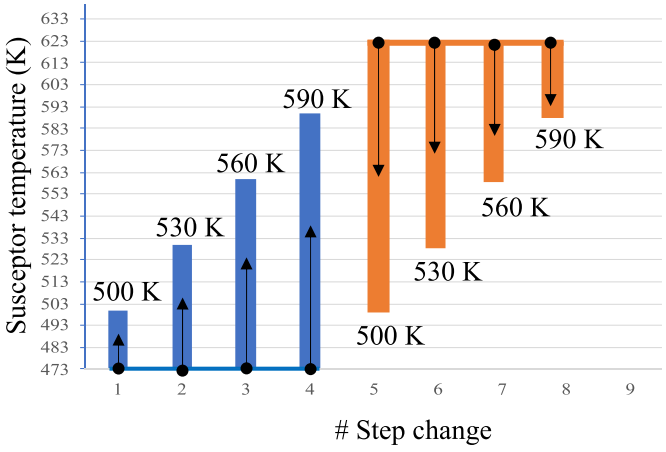

Fig. 6. Step changes of susceptor temperature applied for snapshot collection. Blue bars correspond to temperature increases and orange bars to temperature decreases.

The model order reduction methodology implemented here, is presented in detail in (Koronaki et al., 2017; Gkinis et al. 2017b; Gkinis et al., 2019) and is summarized in this work for completeness.

5.1. Data collection for building the ROM

The first step in the ROM workflow is the collection of data, here vectors containing the distribution of velocity, pressure and temperature at each point in the spatial discretization. To collect these distributions, step changes are applied, to the susceptor temperature, a critical process parameter, as shown schematically in Fig. 6. The blue bars correspond step increases of temperature (common starting point, T=473 K) and the orange bars correspond step decreases of susceptor temperature (common starting point, T=623 K). The choice of applied step changes to the temperature value is based on the actual experimental conditions for which the data are available. Therefore, within a temperature range 473<T<633, several “snapshots” are collected from time-dependent simulations at a fixed time interval Δt=0.1s. The “snapshots” in this case are the vectors containing the distributions of

variables in the reactor, as the system changes in response to the applied step change until it finally reaches a new steady state. Eventually the N × k matrix **S** is assembled, where N is the number of degrees of freedom and k is the total number of instantaneous vectors collected along the trajectories resulting from the different step changes.

Given the fact, that detailed 3D simulations entail a large number of degrees of freedom, it becomes obvious that the computational cost associated with the data collection is not trivial. In this case study, harvesting the data with the detailed 3D model would require more than 20 days in CPU time. Even then, manipulating the resulting data/snapshots would also be a daunting task.

In order to circumvent this problem and render the proposed workflow more applicable in realistic problems, the size of the CFD model is purposefully reduced by using a coarser discretization consisting of 309k finite volumes. As a result, the accuracy of the CFD solution is sacrificed for the sake of efficiency but as it will discussed further on, it can be recovered. Here the discretization is reduced to one third of the "appropriate" one, which led to 1.2 million degrees of freedom. The computational cost of each simulation is 2 CPU hours in 12 cores and the computational cost of deriving the entire data set was 48 CPU hours.

Another important aspect of the ROM that contributes to its computational efficiency, is the fact that chemical reactions and chemical species that participate therein are not included in the simulations conducted for data collection. Therefore, only mass, momentum and energy conservation equations are solved which greatly reduces the required computational effort. This is done based on the fact that the mixture of incoming gases contains a very small amount of precursor (typically around 0.001%). The fact that it is so dilute means that precursor depletion and by-product production does affect the overall gas flow or temperature distribution.

With those considerations in mind, the ROM will be able to give very quick coarse predictions of the flow, precursor mass fraction and energy distributions inside the reactor. The augmentation of this prediction with information about the Cu deposition rate will be discussed further on.

5.2. Proper Orthogonal Decomposition basis

Once the data is collected as a N × k matrix **S**, the next step is to derive a low-dimensional description, in this case a basis of the subspace that contains the data. This is achieved by implementing a variant of the POD (Berkooz et al. 1993), the method of snapshots (Sirovich, 1987), which involves the singular value decomposition (SVD) of the matrix $\mathbf{S} = \mathbf{U}\,\mathbf{\Sigma}\,\mathbf{V}^{\mathrm{T}}$, where **U** and **V** are unitary matrices and **Σ** is diagonal. Nevertheless, the data matrix is usually composed of vectors containing more degrees of freedom than snapshots (N>>k) and it is therefore more efficient to address a small eigenvalue problem:

$$\mathbf{S}^{\mathrm{T}}\mathbf{S}\boldsymbol{\varphi}_{\mathrm{j}} = \lambda_{\mathrm{j}}\boldsymbol{\varphi}_{\mathrm{j}},\ \text{for j} = 1,\ldots,\mathrm{k} \tag{1}$$

the product $\mathbf{S}^{\mathrm{T}}\mathbf{S}$ is the k × k covariance matrix $\mathbf{K} = \mathbf{S}^{\mathrm{T}}\mathbf{S}$, of the assembled data. It holds that:

$$\mathbf{S}^{\mathrm{T}}\mathbf{S} \;=\; \mathbf{V}\,\mathbf{\Sigma}^{2}\,\mathbf{V}^{\mathrm{T}} \Leftrightarrow \left(\mathbf{S}^{\mathrm{T}}\mathbf{S}\right)\mathbf{V} \;=\; \mathbf{V}\,\mathbf{\Sigma}^{2} \tag{2}$$

Which shows that the right singular vectors of **S** are equal to the eigenvectors of the covariance matrix and that the singular values of **S** are the positive square roots of the eigenvalues of **K**.

The m most energetic modes that correspond to 99% of the energy of the data matrix are selected in order to build a low dimensional basis that accurately represents the data matrix. The energy, ε_{j}, of $\boldsymbol{\varphi}_{\mathrm{j}}$ is computed as

$$\varepsilon_j = \frac{\sum_{i=1}^{j}\phi_i}{\sum_{i=1}^{k}\phi_i} \tag{3}$$

Eventually the selected basis is formed as $\mathbf{Z} = [\mathbf{z}_1, \mathbf{z}_2, \ldots, \mathbf{z}_{\mathrm{m}}] \in \Re^{\mathrm{m}\times\mathrm{k}}$, where each column $\mathbf{z}_{\mathrm{i}}$ is computed as

$$\mathbf{z}_{\mathrm{i}} = \frac{1}{\sqrt{\lambda_{\mathrm{i}}}}\sum_{\mathrm{l}=1}^{\mathrm{k}}(\phi_{\mathrm{i}})_{\mathrm{l}}\mathbf{S}_{(\cdot,\mathrm{l})},\ \ 1 \le \mathrm{i} \le \mathrm{m} \tag{4}$$

where $(\phi_{\mathrm{i}})_{\mathrm{l}}$ is the l-th component of the i-th eigenvector $\mathbf{z}_{\mathrm{i}}$ of **K** and $\mathbf{S}_{(\cdot,\mathrm{l})}$ is the l-th column of **S**.

Each column vector $\mathbf{s}_{\mathrm{i}}$ of $\mathbf{S} = [\mathbf{s}_1, \mathbf{s}_2, \ldots, \mathbf{s}_{\mathrm{k}}]$ can be approximated by a linear combination of the form:

$$\mathbf{s}_i^{'} = \mathbf{Z}\alpha_{\mathrm{i}}, \tag{5}$$

where $\boldsymbol{\alpha}_{\mathrm{i}} = [\alpha_{\mathrm{i1}}, \alpha_{\mathrm{i2}}, \ldots, \alpha_{\mathrm{im}}]$ are time-dependent coefficients which describe the time dependency of the data respectively.

Therefore, in order to obtain an accurate low dimensional representation of the data, given a low dimensional basis, **Z**, the coefficients $\boldsymbol{\alpha}_{\mathrm{i}}$ are required. Typically, an ordinary differential equation governing the coefficients $\boldsymbol{\alpha}$, is obtained by substituting the low-order approximation $\mathbf{s}_i'$ to the governing equations (here the conservation equation for mass, momentum and energy) and the projecting onto the subspace spanned by the modes $\mathbf{Z}_{\mathrm{i}}$. In the following paragraph an alternative is presented that circumvents the manipulation of equations by implementing machine learning strategies.

5.3. Prediction of coefficients with Artificial Neural Networks

Artificial Neural Networks (ANNs) are computational algorithms based on statistical principles and are widely applied in areas such Artificial Intelligence, Machine Learning and Data Mining. In this work the nonlinear autoregressive network with external inputs nonlinear autoregressive network with exogenous inputs (NARX) is used (Xie et al., 2009, 2012, 2015). This particular dynamic network has a simpler structure than other known networks with feedback, but is very powerful, converges faster and is better suited for data from time-series. The NARX network can be described by the following expression:

$$\mathrm{y}\ (\mathrm{tk}) \;= F\left(x\left(t_{k-n_x}\right),\ldots,\ x(t_{k-1}), x(t_k), y\left(t_{k-n_y}\right),\ldots,\ y(t_{k-1})\right) \tag{6}$$

i.e., the output y of the system at time t_{k} depends on the input x at the same time as well as on the inputs and outputs of previous times. The parameters n_x and n_y are delays between the input and the output, respectively and practically define the number of past time steps that affect the current output.

Eventually, setting the network input and output delays to one, the output is expressed as:

$$\mathrm{y}\ (\mathrm{tk}) \;= F(x(t_{k-1}), x(t_k), y(t_{k-1})) \tag{7}$$

Finally, the nonlinear function *F* is determined through the training of the dynamic network by known dynamic responses of the reactor to specific step inputs of the mass flow inlet which constitutes the so-called series-parallel implementation of the ANN: whereas in the standard NARX architecture the output of the feed-forward network is used as input, in the series-parallel strategy, the *actual* outputs are used as feedback. This is shown schematically in Fig. 7.

The backpropagation training method, combined with the Levenberg–Marquardt regularization algorithm, is implemented in order to achieve smooth convergence to a low training error, avoiding overfitting. The mean square error, i.e. the averaged squared difference between the input and inferred values is used as performance function, in order to assess the training of the network.

In this implementation, the number of hidden layers is set to 1 with 5 neurons. An overview of the network parameters is presented Table 3. and more details about its implementation are discussed in section 6.2.

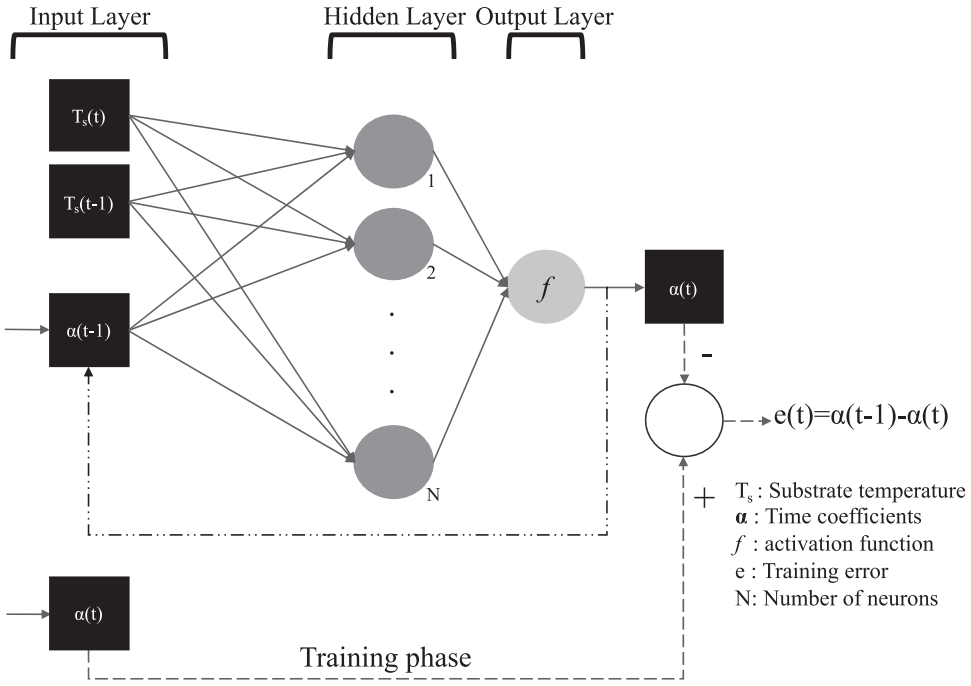

Fig. 7. Structure of the Artificial Neural Network.

Table 3
Overview of specifications of Artificial Neural Network.

ANN specifications	
Type of NN	NARX
Training	Bayesian Regularization Backpropagation
Time delay (n_x,n_y)	1
Activation/Transfer function (f)	Sigmoid
Hidden layer	1
Number of neurons	5

6. Results and discussion

6.1. Reduced order model

The method of snapshots is implemented on a snapshot matrix containing all the data reported in paragraph 5.1 (cf Fig. 6), except for the series of vectors obtained for the step change from 623K to 500K which is retained for testing and validation purposes. Therefore, with one of the eight step changes removed, the snapshot matrix **S** consists of data from seven step changes, with a total number of k=62 snapshots. Each snapshot is a vector of size N=1.86 10^6 containing the values of the velocity components, pressure and temperature at point of the discretization.

Following the methodology presented in paragraph 5.2, 4 POD modes are retained in order to form the low-dimensional basis, **Z**. These represent 98.8% of the energy of the system as defined by equation 3. The variation of the cumulative energy captured by the eigenmodes is presented in Fig. 8. In an effort to demonstrate, the effect of the size of the basis on the accuracy of the predictions, results are presented in the following paragraph, for gradually increasing basis size ranging from 1 to 4 POD modes.

6.2. ANN predictions

Subsequently, the trained Artificial Neural Network (ANN) is used in order to determine the value of the time-dependent coefficients $\boldsymbol{\alpha}_i$ involved in equation 5. The input data consists of the initial condition, i.e. the vector containing the distribution of velocity, pressure and temperature at the initial value of the susceptor temperature. The initial and final value of the temperature in the step change are also included. The output of the network includes the predictions of the time-dependent coefficients $\boldsymbol{\alpha}_i$, that correspond to the snapshots along the trajectory from the state at the initial temperature to the final one. By implementing equation 5, it is possible to reconstruct the entire state vector and compare with the actual values.

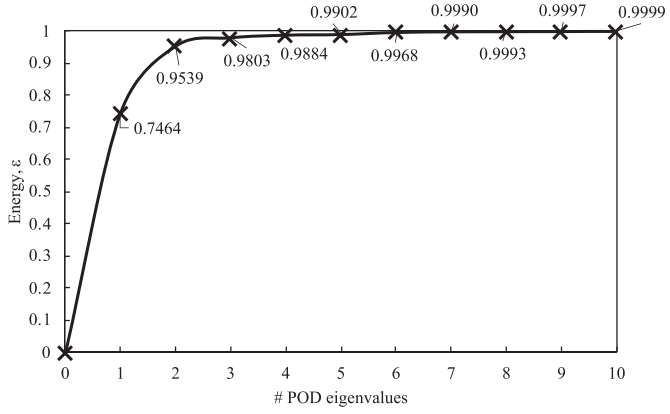

Fig. 8. Energy contained by POD modes. The first four are retained for the ROM, corresponding to 98.8% of the energy of the system.

This comparison is carried out for all four predictive models (one for each POD basis), with increasing size of basis **Z**. The deviation from the actual states, computed with the CFD code, is defined as

$$\boldsymbol{e_i} = \frac{\left\| \boldsymbol{s_i} - \boldsymbol{s_i'} \right\|}{\left\| \boldsymbol{s_i} \right\|} \tag{8}$$

where i is the snapshot number, $\boldsymbol{s_i}$ and $\boldsymbol{s_i'}$ are the CFD calculated and ROM approximated snapshots respectively. The approximation error for the test data set is shown in Fig. 9. There is a decreasing trend in the approximation error, as the size of the POD increases,

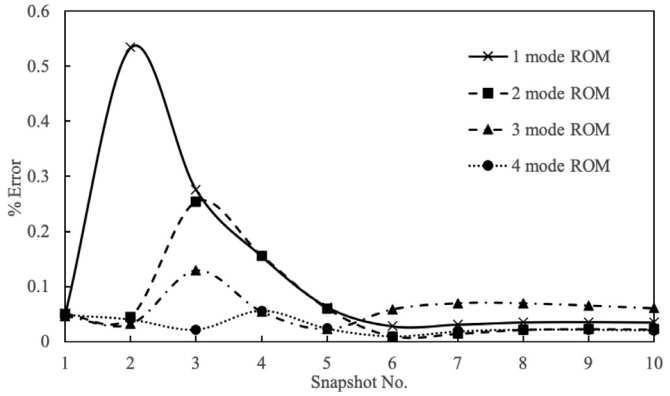

Fig. 9. Error between the ROM estimations and known CFD results (snapshots) along a trajectory that was not included in the training set of the ANN.

nevertheless, in all cases the error is well under 1%, which shows a good generalization capacity of the model, regardless of the basis size. All results shown henceforth are produced with a predictive model involving 3 POD modes, in an effort to boost accuracy without the efficiency of the methodology as a ROM of order 3 entails a very small computational cost.

In order to recover the accuracy lost due to the coarse data that the ROM is based on, it is necessary to "fine-tune" the prediction from the POD/ANN model by feeding them as initial estimates to a detailed CFD model with refined discretization. Due to the fact that the initial estimate of the solution provided by the ROM is a close to the actual one, only a few iterations of the high-fidelity CFD code are required for convergence. The initialization of the CFD code with the results from a coarse mesh, requires the so-called mesh-to-mesh interpolation, here zeroth order (or "nearest neighbor") interpolation, in order to "translate" the prediction to the fine mesh and use it as a preconditioner. During this step, the value of the variables in the fine mesh are set equal to their value in the nearest "coarse-mesh" neighbor.

The computational cost reduction can be calculated in core time, which is the time needed for the CFD computation multiplied by the number of CPU cores used in parallel. Therefore, a single CFD computation of the detailed CFD model (fine mesh and chemical reactions) in parallel with 12 CPU cores requires roughly 864 core hours. While the reduced order model computes an approximation of the solution in less than a minute with a single CPU core, with a further 18 core hours (12 CPU cores) for the detailed model to generate the solution, after being initialized with the ROM approximation. Thus, an acceleration of 4 times in core time is achieved. These results are summarized in Table 4. Considering that this model has to be executed several times for different kinetic constants during the fitting procedure, the overall computational cost reduction is even greater and the benefit from this approach increases with the number of unknown constants.

Table 4
Comparison or required CPU hours.

	Wall clock	CPU hours
Detailed 3D CFD model with reactions	72 hours @12 cores	864 core hours
ROM based on coarse CFD results	18 hours @ 12cores	216 core hours
Acceleration	× 4	

6.3. Chemical reaction parameters

Fitting of the kinetic parameters involves solving the accelerated CFD model for different combination of the constants at the temperatures where the experimental data are available (c.f. Fig. 2). The predicted values of the deposition rate are then compared to the actual values determined experimentally (Fig. 10 bottom) and the process is repeated until the computed predictions converge to the experimental measurements within a tolerance.

A feature of this implementation that further enhances the efficiency of the computational workflow, is that the species mass fractions are not part of the ROM. Instead, chemical reactions are included only in the detailed CFD model. This is made possible by the fact that species depletion or production does not influence the flow in the reactor chamber, because a very dilute gas phase mixture is involved. Therefore, for each new set of kinetic parameters, the detailed CFD model is initialized with the same ROM prediction for the flow and energy distributions. Under the assumption that the flow is unchanged regardless of the kinetic model, the detailed CFD model need only compute corrections for the species concentrations, which requires much less effort than the overall simulation.

The values of the three pre-exponential factors, determined with the help of the computational tool are summarized in Table 5. The deposition rate prediction of the model is compared to the experimental data in the Arrhenius plot shown in Fig. 11. The proposed chemistry model captures accurately the trend of the data, even in temperatures higher than 573K.

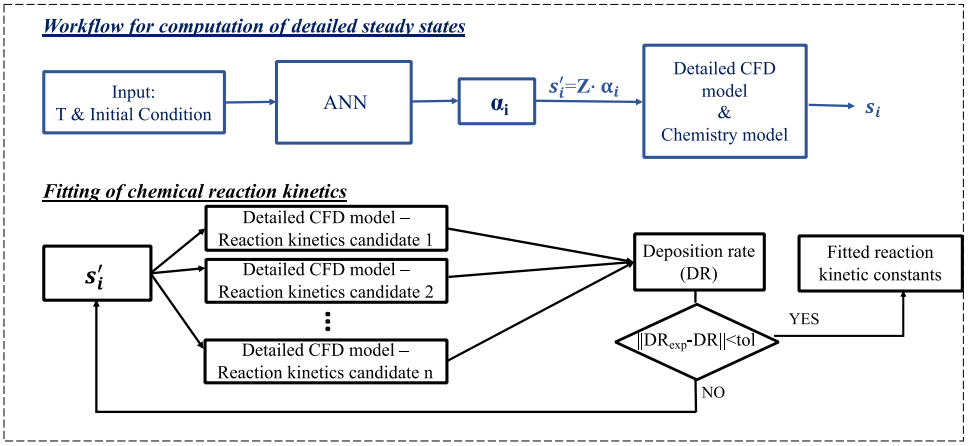

Fig. 10. Schematic of the workflow for the production of detailed steady state predictions for the computation of the deposition rate (DR) (top). Workflow of the kinetic parameters fitting process (bottom).

Table 5
Fitted pre-exponential factors of the chemical reaction system.

Reaction	Pre-exponential factor
Deposition reaction	$1.35{\cdot}10^{10}$ m^3 $kmol^{-1}$ s^{-1}
Carbodiimide deinsertion	$8.5{\cdot}10^{8}$ s^{-1}
β-hydrogen abstraction	$8.5{\cdot}10^{8}$ s^{-1}

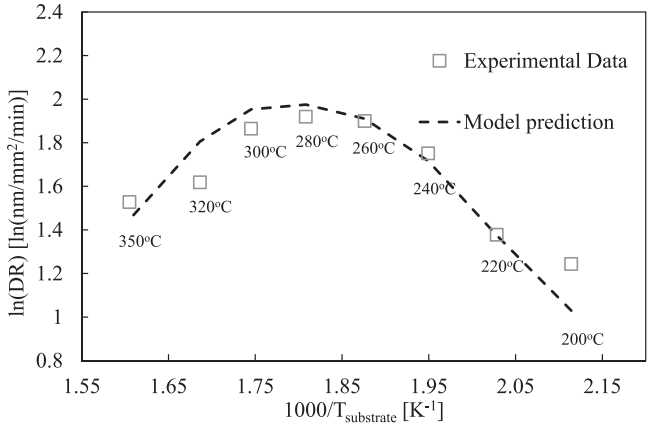

Fig. 11. Comparison of Cu deposition rate, between the fitted chemical reaction system and the experimental data.

7. Conclusions

A new chemistry model is proposed, for the CVD of Cu from Cu amidinate. The innovative aspect is the inclusion of two gas phase reactions, with high activation energy, that capture the sharp decrease of the deposition rate at temperatures above 573K, as a result of precursor depletion. Two mechanisms for Cu amidinate are considered, carbodiimide deinsertion and β-hydrogen abstraction, based on the literature regarding Cu amidinate and a structurally similar precursor, Cu guanidinate.

The kinetic parameters of the proposed chemical pathway are determined by comparing predictions from a machine-learning-assisted CFD model with experimental measurements. This fitting process is computationally expensive and, in this case, becomes feasible by combining reduced order modeling via Proper Orthogonal Decomposition and Artificial Neural Networks. Further savings are achieved by using low-fidelity data, from coarse-mesh CFD simulations, to build the ROM. Accuracy is then recovered by using the ROM prediction as a preconditioner for the detailed CFD model in order to accelerate its convergence. Furthermore, the chemistry model is included only in the detailed CFD model, making the predictive ROM even more efficient.

Declaration of Competing Interest

The authors declare that they have no known competing financial interests or personal relationships that could have appeared to influence the work reported in this paper.

Acknowledgements

The authors would like to thank Dr. Constantin Vahlas (CIRIMAT, CNRS, Université de Toulouse) for providing additional experimental measurements. Dr. E D. Koronaki is supported by the Fonds National de la Recherche (FNR) Luxembourg (HybridSimCVD/14302626). Mr. R. Spencer and Dr. D.I Gerogiorgis gratefully acknowledge financial support of Erasmus+ Student and Teaching Exchange Travel Scholarships from the University of Edinburgh to the National Technical University of Athens (NTUA). Dr. D. I. Gerogiorgis also acknowledges a recent Royal Academy of Engineering (RAEng) Industrial Fellowship, and a current Royal Society (RS) Short Industrial Fellowship.. Mr P. Gkinis acknowledges the financial support by the NTUA Research Committee. Prof. S.P.A. Bordas received funding from the European Union's Horizon 2020 research and innovation program under grant agreement No 811099 TWINNING Project DRIVEN for the University of Luxembourg.

References

Alshehri, A.S., Gani, R., You, F., 2020. Deep learning and knowledge-based methods for computer-aided molecular design—toward a unified approach: State-of-the-art and future directions. Comput. Chem. Eng. 141, 107005. doi:10.1016/j.compchemeng.2020.107005.

Aviziotis, I.G., Cheimarios, N., Vahlas, C., Boudouvis, A.G., 2013. Experimental and computational investigation of chemical vapor deposition of Cu from Cu amidinate. Surface and Coatings Technology 230, 273. doi:10.1016/j.surfcoat.2013.06.014.

Barry, S.T., 2013. Amidinates, guanidinates and iminopyrrolidinates: Understanding precursor t0hermolysis to design a better ligand. Coord. Chem. Rev. 257, 3192–3201. doi:10.1016/j.ccr.2013.03.015.

Berkooz, G., Holmes, P., Lumley, J.L., 1993. The proper orthogonal decomposition in the analysis of turbulent flows. Annu. Rev. Fluid Mech. 25, 539–575. doi:10.1146/annurev.fl.25.010193.002543.

Bracconi, M., Maestri, M., 2020. Training set design for machine learning techniques applied to the approximation of computationally intensive first-principles kinetic models. Chem. Eng. J. 400, 125469. doi:10.1016/j.cej.2020.125469.

Chen, L., Pannala, S., Broekhuis, R., Gautam, P., Gu, T., West, D., Balakotaiah, V., 2020. Three-dimensional CFD simulation of pattern formation in a shallow packed-bed reactor for oxidative coupling of methane. Chem. Eng. J. 400, 125979. doi:10.1016/j.cej.2020.125979.

Chen, X., Yao, J., Jiang, S.C., Liu, C., Guo, M., Gao, N., Zhang, Z., 2020. An improved CFD modeling approach applied for the simulation of gas–liquid interaction in the ozone contactor along with structure optimization. Chem. Eng. J. 384, 123322. doi:10.1016/j.cej.2019.123322.

Clayton, A.D., Schweidtmann, A.M., Clemens, G., Manson, J.A., Taylor, C.J., Niño, C.G., Chamberlain, T.W., Kapur, N., Blacker, A.J., Lapkin, A.A., Bourne, R.A., 2020. Automated self-optimisation of multi-step reaction and separation processes using machine learning. Chem. Eng. J. 384, 123340. doi:10.1016/j.cej.2019.123340.

Coyle, J.P., Johnson, P.A., DiLabio, G.A., Barry, S.T., Müller, J., 2010. Gas-Phase Thermolysis of a Guanidinate Precursor of Copper Studied by Matrix Isolation, Time-of-Flight Mass Spectrometry, and Computational Chemistry. Inorg. Chem. 49, 2844–2850. doi:10.1021/ic902247w.

Coyle, J.P., Kurek, A., Pallister, P.J., Sirianni, E.R., Yap, G.P.A., Barry, S.T., 2012. Preventing thermolysis: precursor design for volatile copper compounds. Chem. Commun. 48, 10440. doi:10.1039/C2CC35415B.

Dey, S., Dhar, A., 2020. On proper orthogonal decomposition (POD) based reduced-order modeling of groundwater flow through heterogeneous porous media with point source singularity. Adv. Water Resour. 144, 103703. doi:10.1016/j.advwatres.2020.103703.

Gao, X., Li, T., Rogers, W.A., Smith, K., Gaston, K., Wiggins, G., Parks, J.E., 2020. Validation and application of a multiphase CFD model for hydrodynamics, temperature field and RTD simulation in a pilot-scale biomass pyrolysis vapor phase upgrading reactor. Chem. Eng. J. 388, 124279. doi:10.1016/j.cej.2020.124279.

Gkinis, P.A., Aviziotis, I.G., Koronaki, E.D., Gakis, G.P., Boudouvis, A.G., 2017. The effects of flow multiplicity on GaN deposition in a rotating disk CVD reactor. J. Cryst. Growth 458, 140. doi:10.1016/j.jcrysgro.2016.10.065.

Gkinis, P.A., Koronaki, E.D., Skouteris, A., Aviziotis, I.G., Boudouvis, A.G., 2019. Building a data-driven Reduced Order Model of a Chemical Vapor Deposition process from low-fidelity CFD simulations. Chem. Eng. Sci. 199, 371. doi:10.1016/j.ces.2019.01.009.

Gkinis, P.A., Aviziotis, I.G., Koronaki, E.D., Gakis, G.P., Boudouvis, A.G., 2017. The effects of flow multiplicity on GaN deposition in a rotating disk CVD reactor. J. Cryst. Growth 458, 140–148. doi:10.1016/j.jcrysgro.2016.10.065.

Gosiewski, K., Pawlaczyk-Kurek, A., 2019. Aerodynamic CFD simulations of experimental and industrial thermal flow reversal reactors. Chem. Eng. J. 373, 1367–1379. doi:10.1016/j.cej.2019.03.274.

Gyurik, L., Ulbert, Z., Molnár, B., Varga, T., Chován, T., Egedy, A., 2020. CFD Based Nozzle Design for a Multijet Mixer. Chem. Eng. Process 157, 108121. doi:10.1016/j.cep.2020.108121.

Hijazi, S., Stabile, G., Mola, A., Rozza, G., 2020. Data-driven POD-Galerkin reduced order model for turbulent flows. J. Comp. Phys. 416, 109513. doi:10.1016/j.jcp.2020.109513.

Kim, M., Park, S., Lee, D., Lim, S., Park, M., Min Lee, J., 2020. Modeling long-time behaviors of industrial multiphase reactors for CO2 capture using CFD-based compartmental model. Chem. Eng. J. 395, 125034. doi:10.1016/j.cej.2020.125034.

Koo, B., Jo, T., Lee, D., 2019. Modified inferential POD/ML for data-driven inverse procedure of steam reformer for 5-kW HT-PEMFC. Comput. Chem. Eng. 121, 375–387. doi:10.1016/j.compchemeng.2018.11.012.

Koronaki, E.D., Nikas, A.M., Boudouvis, A.G., 2020. A data-driven reduced-order model of nonlinear processes based on Diffusion Maps and Artificial Neural Networks. Chem. Eng. J. 397, 125475. doi:10.1016/j.cej.2020.125475.

Koronaki, E.D., Gkinis, P.A., Beex, L., Bordas, S.P.A., Theodoropoulos, C., Boudouvis, A.G., 2019. Classification of states and model order reduction of large scale Chemical Vapor Deposition processes with solution multiplicity. Comput. Chem. Eng. 121, 148–157. doi:10.1016/j.compchemeng.2018.08.023.

Krisyuk, V.V., Aloui, L., Prud'homme, N., Sarapata, B., Senocq, F., Samélor, D., Vahlas, C., 2009. CVD of Pure Copper Films from a Novel Amidinate Precursor. ECS Trans. 25, 581–586. doi:10.1149/1.3207643.

Lee, J.H., Shin, J., Realff, M.J., 2018. Machine learning: overview of the recent progresses and implications for the process systems engineering field. Comput. Chem. Eng. 114, 111–121. doi:10.1016/j.compchemeng.2017.10.008.

Li, K., Huang, T.-Z., Lanteri, L., Li, S., 2019. POD-based model order reduction with an adaptive snapshot selection for a discontinuous Galerkin approximation of the time-domain Maxwell's equations. J. Comp. Phys. 396, 106–128. doi:10.1016/j.jcp.2019.05.051.

Lim, B.S., Rahtu, A., Gordon, R.G., 2003. Atomic layer deposition of transition metals. Nat. Mater. 2, 749–754. doi:10.1038/nmat1000.

Lira, J.O.B., Riella, H.G., Padoin, N., Soares, C., 2020. CFD + DoE optimization of a flat plate photocatalytic reactor applied to NOx abatement. Chem. Eng. Process 154, 107998. doi:10.1016/j.cep.2020.107998.

Massmann, T., Kocks, C., Parakenings, L., Weber, B., Jupke, A., 2020. Two-Dimensional CFD based compartment modeling for dynamic simulation of semi-batch crystallization processes in stirred tank reactors. Comput. Chem. Eng. 140, 106933. doi:10.1016/j.compchemeng.2020.106933.

Mayangsari, T.R., Lamierza Yusup, L., Hidayat, R., Chowdhury, T., Kwon, Y.-K., Lee, W.-J., 2021. Reactivity of different nitriding agents with chlorine-terminated surface during atomic layer deposition of silicon nitride. Appl. Surf. Sci. 535, 147727. doi:10.1016/j.apsusc.2020.147727.

Mwema, F.M., Oladijo, O.P., Akinlabi, S.A., Akinlabi, E.T., 2018. Properties of physically deposited thin aluminium film coatings: a review. J. Alloys Compd. 747, 306–323. doi:10.1016/j.jallcom.2018.03.006.

Narasingam, A., Sang-Il Kwon, J., 2018. Data-driven identification of interpretable reduced-order models using sparse regression. Comput. Chem. Eng. 119, 101–111. doi:10.1016/j.compchemeng.2018.08.010.

Nishikawa, T., Horiuchi, K., Joutsuka, T., Yamauchi, S., 2020. Low-pressure chemical vapor deposition of Cu on Ru using CuI as precursor. J. Cryst. Growth 549, 125849. doi:10.1016/j.jcrysgro.2020.125849.

Panzeri, G., Dell'Oro, R., Trifiletti, V., Parravicini, J., Acciarri, M., Binetti, S., Magagnin, L., 2019. Copper electrodeposition onto zinc for the synthesis of kesterite Cu2ZnSnS4 from a Mo/Zn/Cu/Sn precursor stack. Electrochem. Commun. 109, 106580. doi:10.1016/j.elecom.2019.106580.

Prud'homme, N., Constantoudis, V., Turgambaeva, A.E., Krisyuk, V.V., Samélor, D., Senocq, F., Vahlas, C., 2020. Chemical vapor deposition of Cu films from copper(I) cyclopentadienyl triethylphophine: Precursor characteristics and interplay between growth parameters and films morphology. Thin Solid Films 701, 137967. doi:10.1016/j.tsf.2020.137967.

Rasadujjaman, M., Watanabe, M., Sudoh, H., Machida, H., Kondoh, E., 2015. Supercritical fluid chemical deposition of Cu in Ru and TiN-lined deep nanotrenches using a new Cu(I) amidinate precursor. Microelectron. Eng. 137, 32–36. doi:10.1016/j.mee.2014.11.021.

Sharif, S., Ahmad, K.S., 2020. Synthesis of palladium diethyldithiocarbamate complexes as precursor for the deposition of un-doped and copper sulfide doped thin films by a facile physical vapour deposition technique. Optik 218, 165014. doi:10.1016/j.ijleo.2020.165014.

Shi, J., Gourma, M., Yeung, H., 2021. A CFD study on horizontal oil-water flow with high viscosity ratio. Chem. Eng. Sci. 229, 116097. doi:10.1016/j.ces.2020.116097.

Sipp, D., Fosas de Pando, M., Schmid, P.J., 2020. Nonlinear model reduction: A comparison between POD-Galerkin and POD-DEIM methods. Comput. Fluids 208, 104628. doi:10.1016/j.compfluid.2020.104628.

Sirovich, L., 1987. Turbulence and the dynamics of coherent structures. I—III. Quart. Appl. Math. 45, 561–590. doi:10.1090/qam/910464.

Stluka, P., Mařík, K., 2007. Data-driven decision support and its applications in the process industries. Editor(s): Valentin Pleşu, Paul Şerban Agachi. Comput. Aided Chem. Eng. 24, 273–278. doi:10.1016/S1570-7946(07)80069-1.

Tanaka, K., Yanashima, H., Yako, T., Kamio, K., Sugai, K., Kishida, S., 2001. Aluminum chemical vapor deposition reaction of dimethylaluminum hydride on TiN studied by X-ray photoelectron spectroscopy and time-of-flight secondary ion mass spectrometry. Appl. Surf. Sci. 171, 71–81. doi:10.1016/S0169-4332(00)00542-0.

Turgambaeva, A., Prud'homme, N., Krisyuk, V., Vahlas, C., 2011. Decomposition Schemes of Copper(I) N,N ′ -Diisopropylacetamidinate During Chemical Vapor Deposition of Copper. J. Nanosci. Nanotechnol. 11, 8198–8201.

Wang, Y., Ma, H., Cai, W., Zhang, H., Cheng, J., Zheng, X., 2020. A POD-Galerkin reduced-order model for two-dimensional Rayleigh-Bénard convection with viscoelastic fluid. Int. Commun. Heat Mass Transf. 117, 104747. doi:10.1016/j.icheatmasstransfer.2020.104747.

Xie, H., Tang, H., Liao, Y.-H., 2009. Time series prediction based on NARX neural networks: An advanced approach. In: Proceedings of the Eighth International Conference on Machine Learning and Cybernetics. Baoding.

Xie, W., Bonis, I., Theodoropoulos, C., 2012. Linear MPC based on data-driven Artificial Neural Networks for large-scale nonlinear distributed parameter systems. Editor(s): Ian David Lockhart Bogle, Michael Fairweather. Comput. Aided Chem. Eng. 30, 1212–1216.

Xie, W., Bonis, I., Theodoropoulos, C., 2015. Data-driven model reduction-based nonlinear MPC for large-scale distributed parameter systems. J. Proc. Control. 35, 50–58. doi:10.1016/j.jprocont.2015.07.009.

Yan, Y., Mattisson, T., Moldenhauer, P., Anthony, E.J., Clough, P.T., 2020. Applying machine learning algorithms in estimating the performance of heterogeneous, multi-component materials as oxygen carriers for chemical-looping processes. Chem. Eng. J. 387, 124072. doi:10.1016/j.cej.2020.124072.

Zhu, X., Wan, Z., Tsang, D.C.W., He, M., Hou, D., Su, Z., Shang, J., 2021. Machine learning for the selection of carbon-based materials for tetracycline and sulfamethoxazole adsorption. Chem. Eng. J. 406, 126782. doi:10.1016/j.cej.2020.126782.